Journal of
Ceramic Science
and Technology

J. Ceram. Sci. Tech., **04** [02] 77-84 (2013)
DOI: 10.4416/JCST2012-00039a
available online at: http://www.ceramic-science.com

Synthesis, Characterization and Luminescence Properties of Pr^{3+}-Doped C12A7 and C3A

E. Tõldsepp*, E. Feldbach, M. Kirm

Institute of Physics, University of Tartu, Riia 142, Tartu, Estonia
received September 28, 2012; received in revised form November 27, 2012; accepted Januar 16, 2013

Abstract

This paper presents comparative results of luminescence studies on complex wide-band-gap calcium aluminates $12CaO{\cdot}7Al_2O_3$ (C12A7, E_g~7.0 eV) and $3CaO{\cdot}Al_2O_3$ (C3A, E_g~6.5 eV) doped with Pr^{3+} ions. Doped C12A7 ceramics and C3A powders were prepared via self-propagating combustion synthesis followed by different thermal treatments. Time-resolved VUV spectroscopy of C3A:Pr^{3+} revealed fast interconfigurational 5d-4f emission of Pr^{3+} in the region of 3 eV – 4.5 eV with lifetimes of ~ 17 ns upon direct excitation of Pr^{3+} 5d levels, and ~ 30 ns upon interband transitions. Acceleration of decay times (~ 12 – 13 ns) were observed upon XUV excitation at 130 eV. In C3A, multiple non-equivalent lattice sites for Pr^{3+} ions were identified. The energy transfer from host to Pr^{3+} 5d states is inefficient, particularly in C12A7, where the separation of 5d-4f transitions from other competing luminescence channels is not straightforward owing to the complexity of the host crystal band structure. The slow intraconfigurational 4f-4f emission originating from the second stage of 4f cascade was observed for both compounds.

Keywords: Calcium aluminate, C12A7, C3A, praseodymium, VUV spectroscopy

I. Introduction

Pr^{3+}-doped inorganic materials are widely studied for their potential applications as scintillation materials owing to the fast Pr^{3+} 5d-4f emission (~ 7 – 30 ns), as quantum-cutting phosphors exhibiting photon cascade emission [1,2], and as long afterglow phosphors. Several garnets and alkaline earth aluminates [3–5] have shown promising properties for the above-mentioned applications. Ceramic materials are widely used in optical applications because in comparison with single crystals their production costs are lower, their manufacturing process simpler and there are almost no limits on shaping the material to the form required for application. In addition, the optical properties of dense ceramics are homogeneous, which is an advantage over polycrystalline powders or single crystals with preferential direction.

In this paper, we present luminescence studies on Pr^{3+}-doped calcium aluminates $12CaO{\cdot}7Al_2O_3$ (C12A7) and $Ca_3Al_2O_6$ (C3A) with a cubic crystal structure. C12A7 has attracted a great deal of attention because of its unique crystal and band structures as these enable the formation of stable inorganic electride [6]. The unit cell of C12A7 (cubic, I-43d, Z = 2, a = 11.99 Å) consists of twelve positively charged (1/3+ per cage) interconnected cages with inner free space of 4 Å in diameter. The charge neutrality of stoichiometric C12A7 is achieved by O^{2-} anions inside 1/6 of the cages, which can also act as charge compensators when an extra charge is introduced into the lattice. With different chemical treatments, extra-framework O^{2-} anions can be replaced by various anions with higher concentrations than ordinary defects in solids [7]. A large number of positively charged cages present in the crystal structure modifies the band structure and results in an additional narrow conduction band referred to as the cage conduction band (CCB), which is located ~ 2 eV below the bottom of the framework conduction band. Recent experimental photoemission studies have located its position from 5 to 6.2 eV from the top of the valence band [8]. However, so far no spectroscopic evidence exists, which could be attributed to recombination of the encaged electrons with holes resulting in light emission. Moreover, according to theoretical calculations the occupied cage level is located below the CCB by 0.6 – 1.1 eV [9], which shifts potential emission to lower energies. The band structure is even more complex as the energy levels of specific extra-framework anions can appear in the band gap [7]. Also, there are two non-equivalent Ca^{2+} sites in every cage. Different extra-framework anions cause additional deformation of the cages in which they are placed, leading to symmetry reduction, but the variety of possibilities for modification of the host properties makes C12A7 suitable for studying luminescence properties dependent on extra-framework species.

The C3A consists of the same chemical elements as C12A7, which contribute to the formation of the electronic structure. However, the structure of C3A (cubic, Pa3, Z = 24, a = 15.26 Å) contains a larger number of non-equivalent Ca^{2+} sites compared to C12A7, i.e. six per unit cell. Three Ca^{2+} sites have coordination number 6 (two with a compressed octahedral symmetry, one with

* Corresponding author: eliko.toldsepp@ut.ee

a distorted trigonal prism geometry), and the other three sites have coordination numbers 9, 8 and 7 with more distorted local geometries. The unit cell consists of eight fragments in which six AlO_4 tetrahedra surround a hole with a diameter of 2.94 Å in which Ca^{2+} ions are holding the rings together [10]. 1/9 of holes in the unit cell are not occupied and these Ca^{2+} vacancies are expected to act as charge stabilizers when an extra charge is introduced into the structure [11].

In both of these compounds praseodymium ions are expected to replace Ca^{2+} owing to their similar radii, and the charge compensation in C12A7 and C3A could be realized as described earlier. The 5d levels of Pr^{3+} ions are very sensitive to crystal field strength on the site of substitution showing either a photon cascade of $4f^2$ transitions if $^1S_0$ is the emitting level below 5d states or, in opposite case, the $5d4f^1$ transitions to several low-lying $4f^2$ states. Depending on the host and number of cation sites available, the picture can be more complicated, with both types of emissions being detected depending on the selected excitation energy [12].

Previously, Pr^{3+}-doped $Sr_3Al_2O_3$, which is isostructural with C3A, has been reported as a prospective phosphor material for a UV dosimeter [4]. C12A7 compound doped with various rare earths [13–17]has also been investigated. However, in most of these papers the spectroscopic properties in the UV-visible range are evaluated, which determines the underlying physics. In this paper we present our results obtained from a comparative study on Pr 5d-4f luminescence in C12A7 and C3A hosts upon vacuum ultraviolet (VUV) and extreme ultraviolet (XUV) excitation.

II. Experimental Details

The powders of undoped and Pr^{3+} (0.25 mol%)-doped C3A and C12A7 were prepared by means of self-propagating combustion synthesis, starting from the high-purity materials $Ca(NO_3)2{\cdot}4H_2O$ (99.999 %, Alfa-Aesar), $Al(NO_3)3{\cdot}9H_2O$ (99.99 %, Alfa-Aesar) and $Pr(NO_3)3{\cdot}6H_2O$ (99.99 %, Alfa-Aesar). A stoichiometric mixture of β-alanine and urea was used as fuel, following the fuel mixture approach that considers oxidizing-reducing agent ratios depending on molar ratios of nitrates [18]. The amount of Pr^{3+} (0.25 mol%) ions was chosen in the range where concentration quenching influencing optical properties is not expected. Metal nitrates were dissolved in ~30 mL deionized water followed by the addition of the fuel mixture. The solution was placed into a vertical tube furnace heated to 500 °C. After rapid vaporization of water the combustion process was self-initiated and calcium aluminate powders obtained. The obtained C3A powders were annealed in air at 850 °C for 5 h followed by the phase purity confirmation by means of powder X-ray diffraction (XRD). XRD data was collected using a Rigaku Smartlab diffractometer (Cu Kα radiation, 2θ=10–90°, step 0.01°, integration time 1 s). The C12A7 powders obtained from the combustion reaction were subjected to a melt-solidification process [19] in a carbon crucible followed by slow cooling at a rate of ~400 °C/h in order to favour crystallization. The solidified C12A7 samples had a dark green coloration owing to partial replacement of cage-oxygens by electrons, confirmed by a 2.8 eV band in the absorption spectrum that is typical for C12A7 electride [20]. The obtained C12A7:Pr^{3+} samples were heated in air at 900 °C for 1–3 h. The resulting ceramic objects were transparent and pale green, unlike undoped C12A7 samples, which were colourless after similar treatment. The coloration was found to be present due to Pr^{3+} 4f absorption lines in visible spectral region. The C12A7 samples were characterized using Raman spectroscopy (Renishaw inVia micro-Raman spectrometer, Ar-ion laser, 514 nm) at room temperature. In the Raman spectra of air-treated samples the main Raman frequencies coincided with reported vibrational bands for single-phase C12A7 ceramics [21], confirming that the phase purity of C12A7 samples was suitable for luminescence studies. The morphology of praseodymium-doped samples was examined with scanning electron microscopy (SEM: Philips XL-30 ESEM) as shown in Fig. 1. For the C3A: Pr^{3+} sample (Fig. 1a) agglomerated particles from 0.5 μm to 3 μm were observed, whereas the SEM image of the ceramic C12A7: Pr^{3+} sample (Fig. 1b) indicated that during crystallization dense material with a homogeneous structure was formed.

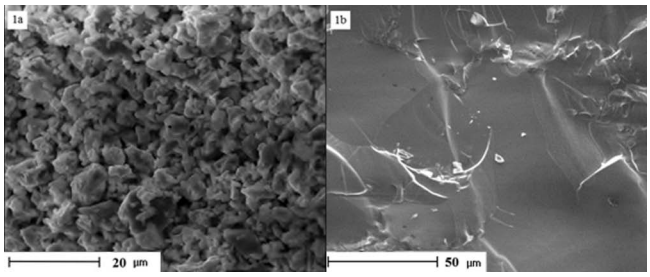

Fig. 1: SEM micrographs of (a) C3A: Pr^{3+} (0.25 mol%) powder and (b) C12A7: Pr^{3+} (0.25 mol%) ceramics.

Time-resolved VUV spectroscopy experiments were performed at the SUPERLUMI station [22] and in XUV at the BW3 beamline [23] of HASYLAB (DESY, Hamburg, Germany) at DORIS storage ring. 10 bunch filling mode was used, which allowed recording of spectra in 100 ns intervals. Spectra were recorded simultaneously in time-integrated mode and in a short- (FTW) and long-time window (STW) with the length of Δt and delayed by the time interval δt relative to the beginning of the synchrotron excitation pulse. The time-correlated single photon counting technique applied is similar in both setups. Such a technique is extremely helpful in distinguishing fast and slow emissions owing to inter- and intraconfigurational transitions (transitions between 4f-5d and 4f-4f states, respectively) of rare earth ions. It is important to point out that the spectral sensitivities of the setups used differ from each other. In the SUPERLUMI setup under VUV excitation (excitation energy range 4–40 eV) we used the UV-visible spectrometer ARC SpectraPro 2300i (operating range 200–1000 nm) equipped with the PMT R6358P (Hamamatsu) having a sensitivity maximum approaching 400 nm. The VUV-optimized monochromator (operating range 60–500 nm) in the Seya-Namioka mounting is used in the luminescence setup at the BW3 beamline (excitation energy range 50–1500 eV) equipped with the MCP 1645 U-09, Hamamatsu microchannel type PMT tube. Therefore, because of differences in the optimization of spectral

devices, UV emissions appear at the shorter wavelengths than in the SUPERLUMI, where the analysing spectrometer is operating in air.

III. Results and Discussion

The spectroscopic investigation of Pr^{3+}-doped calcium aluminates was performed in XUV (Figs. 2 and 3) at 10 K and 300 K; and also in VUV (Figs. 4 to 6) at 10 K in order to distinguish host-related luminescence and parity allowed interconfigurational $4f^15d^1 \rightarrow 4f^2$ emission of Pr^{3+} by means of time-resolved spectroscopy.

Figs. 2a and b show the time-resolved emission spectra of C12A7:Pr^{3+} upon excitation by 130 eV XUV photons measured at 300 K and 10 K, respectively. This energy region starting from 100 eV corresponds to the onset of 4d absorption of rare earth ions known as "giant resonance" (see Ref. [24] and references therein). The emission spectrum (Fig. 2b) recorded at 10 K in time-integrated (TI) mode shows a broad emission band with maximum at 5.2 eV, also dominating in the long-time window (i.e. has a long decay time; STW), which starts 15 ns after excitation with the length of time window 50.1 ns. There are additional broad bands covering the range of 2.7 eV – 3.7 eV with multicomponent decay. At 300 K (Fig. 2a), the emission at 5.2 eV occurs as a shoulder on the high-energy side of a broad emission band with maxima at 4.3 eV and 4.9 eV, both giving a major contribution in the long-time window. For undoped C12A7 the emission bands in the range of 4.0 – 4.5 eV were not observed (not shown). In Ref. [25] the nanosecond emission at ~5 eV in C12A7 electride sample was tentatively assigned to the radiative decay of self-trapped excitons with hole-components localized on framework oxygens. The replacement of the extra-framework oxygen ions with electrons in the electride sample cleans the states due to these ions within the energy gap of C12A7, facilitating observation of self-trapped exciton states. The electron-hole pair formation is needed for this process because the excitation onset coincides with the energy gap. The self-trapping process does not facilitate energy transfer to Pr^{3+} because there is a limited spectral overlap with their absorption starting from 5.2 eV (see Fig. 5a) and a finite migration rate of self-trapped excitons. Another process which may occur is due to the fact that excited electrons can relax to the lower-lying cage polaron states (see Ref. [7, 9]) and the 5.2 eV emission may arise as the result of their recombination with valence band holes. However, there is no experimental evidence from our earlier studies of pure C12A7 to firmly support the latter mechanism. Moreover, these electrons can relax into the occupied cage level, whose energetic position is 0.6 – 1.1 eV below the cage conduction band according to the theoretical calculations [9]. Therefore, the expected emission peak is at lower energies by same value, unless electrons directly from the cage conduction band participate in recombination. It has been extensively discussed for RE-doped oxides [26] that electron hole recombination at rare earth ions is responsible for luminescence. This is the most probable cause for the 5.2 eV emission in C12A7:Pr^{3+}. The comparison of Figs. 2 and 4 shows that UV emission is well pronounced under XUV excitation (130 eV) rather than at the band gap excitation (7 eV). The penetration depth of XUV photons is approximately one order of magnitude higher because of the host absorption coefficients being in order of 10^5 and 10^6 cm^{-1} under the inner shell and near the fundamental absorption edge, respectively. This circumstance explains the role of reabsorption and surface effects, which suppresses weaker intrinsic emissions under VUV excitation in comparison with that of induced dopants like Pr.

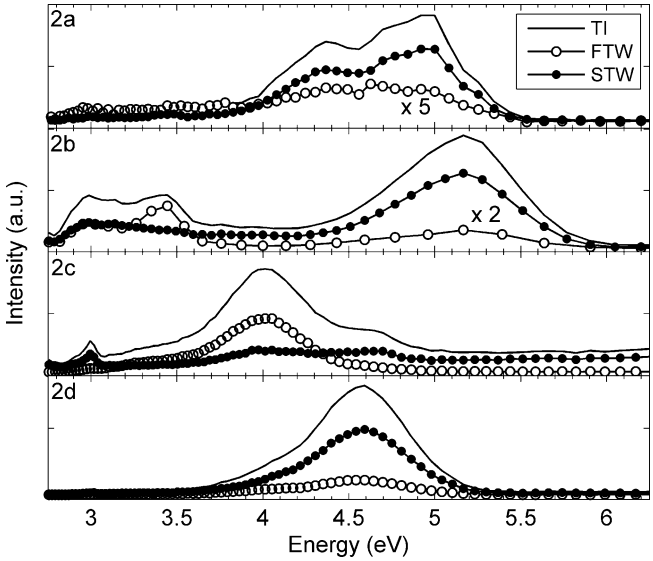

Fig. 2: Emission spectra of C12A7:Pr^{3+} (a, b) and C3A:Pr^{3+} (c, d) at 300 K (a, c) and at 10 K (b, d) upon XUV excitation at 130 eV (FTW: δt = 0 ns, Δt =5.2 ns; STW: δt = 15.0 ns, Δt = 50.1 ns).

It was also discussed in Ref. [25] that the excitation spectrum of 3.3 eV emission starting in the energy gap at 5 eV and strong dependence on the thermochemical treatment of samples providing encaged ions of different types allows the identification of the origin of emission bands. Therefore, the complex luminescence band at lower energies near 3.3 eV is due to the recombination of electrons with holes trapped on extra-framework ions inside the cages (O^{2-} in the stoichiometric case). However, as can be seen in Figs. 2a and b, there are always fast decay components present for 2 – 4 eV emission with lifetimes in the range of 2 – 15 ns, when fitted by two exponential decay and could be assigned as Pr^{3+} 5d-4f emissions. The only fast intrinsic emission with lifetimes 3.7 and 29 ns so far has been observed for 5 eV band in the electron-loaded C12A7 at low temperatures under excitation in host absorption [25].

The emission spectra of C3A:Pr^{3+} upon XUV excitation by 130 eV photons are presented in Figs. 2c and d, at 300 K and 10 K, respectively. At 300 K broad band fast emission with the main maximum at 4.0 eV is observed. This emission is also present at 10 K, but not clearly distinguished owing to the strong 4.6 eV emission dominating in the long-time window spectrum (Fig. 2d). The latter one is assigned to the intrinsic emission as observed in pure C3A sample at the excitation energies above 6.25 eV, which corresponds to the intrinsic absorption of the host. Fig. 2c demonstrates that this UV emission undergoes strong thermal quenching and has long a μs-lifetime, being typical for self-trapped excitons in oxides [27]. The decay curves measured for ~4 eV emission in C3A:Pr^{3+} upon XUV excitation by 130 eV at 10 K and at 300 K are presented

in Fig. 3. The decay curves were fitted with a sum of two exponentials described by time-constants of ~2 ns and ~12 ns at 10 K (curve 1), and ~2 ns and ~7 ns (curve 2) at 300 K. The acceleration of decay components (in comparison to VUV excitation) is a known phenomenon owing to the presence of various competing relaxation channels of electronic excitations (non-radiative decay, photoemission, etc.) as discussed in [24]. In pure and doped calcium aluminates the formation of quenching centres upon high-energy XUV excitation is testified by rather fast decrease of luminescence intensities, especially for C12A7 samples.

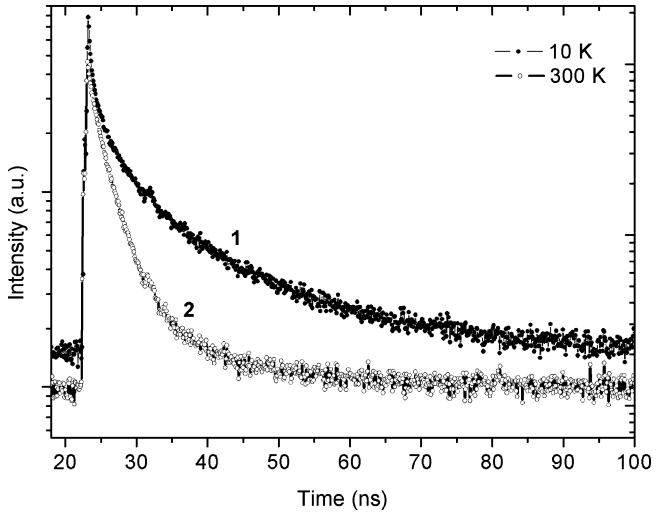

Fig. 3: Luminescence decay curves monitored at 3.87 eV (1) at 10 K and 4.13 eV at 300 K (2) in C3A:Pr^{3+} upon XUV excitation by 130 eV photons.

Under XUV excitation at 300 K in time-integrated and long time-window spectra of C3A:Pr^{3+}, a narrow band at ~3.0 eV was observed, whose spectral position coincides with 4f $^1S_0$ - $^1I_6$ emission, belonging to the first stage in photon cascade emission (PCE). However, it was absent in the emission spectra of C3A:Pr^{3+} upon 5d and interband host (see Fig. 4b) excitation in UV-VUV region, where the second stage of PCE is clearly revealed as a set of 4f-4f transitions. The assignment of ~3 eV emission and possible reasons for the appearance of radiative transitions from $^1S_0$ need further experimental clarification.

Fig. 4 shows the time-resolved emission spectra of C12A7 and C3A doped with 0.25 mol% Pr^{3+} at various excitation energies in VUV at 10 K. The emission spectra of C3A:Pr^{3+} recorded upon excitation in the transparency range of the host at energies 5.14 eV and 6.02 eV at 10 K (Fig. 4b) are dominated by complex broad emission bands between 2.9 eV and 5 eV exhibiting fast decay in the ns range. These emission bands correspond to interconfigurational transitions from the lowest excited state of $4f^15d^1$ configuration to the $4f^2$ ground states of Pr^{3+}. The bands are also observed upon XUV excitation (Fig. 2c and d). In Fig. 5b, the time-integrated excitation spectra of C3A:Pr^{3+} emissions recorded at 3.94 and 3.1 eV show the rich structure of the bands, with weaker luminescence intensity showing maxima at 5.26 eV, 5.62 eV (curve 11) and with stronger intensity at 5.42 eV, 5.96 eV (curve 8). Similar features are observed in the spectra recorded in the short-time window and the emissions have decay in the ns range.

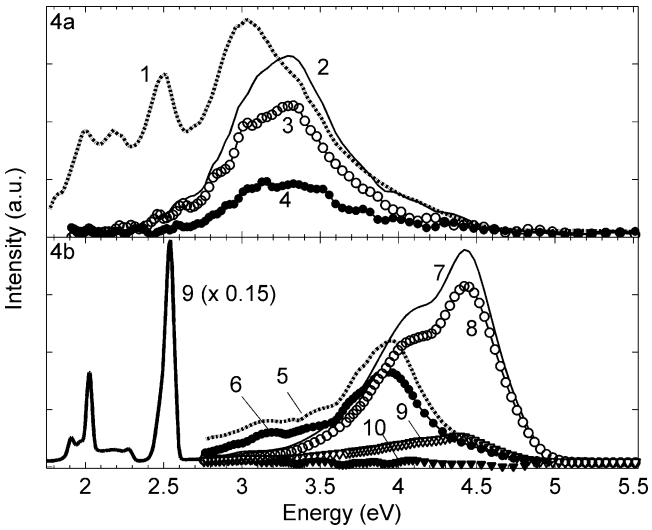

Fig. 4: Emission spectra of (a) C12A7:Pr^{3+} excitation at 7.0 eV (1) and at 6.7 eV (2, 3, 4); and emission spectra of (b) C3A:Pr^{3+} recorded upon excitation at 5.14 eV (5, 6, 10) and at 6.02 eV (7, 8, 9) . Spectra are recorded at 10 K in time-integrated mode (1, 2, 5, 7, 9) and in short- (3, 6, FTW: δt =0.5 ns, Δt = 7.2 ns; 8, FTW: δt = 1.4 ns, Δt = 7.0 ns) and long- (4, 9, 10, STW: δt = 50.3 ns, Δt = 19.2 ns) time windows..

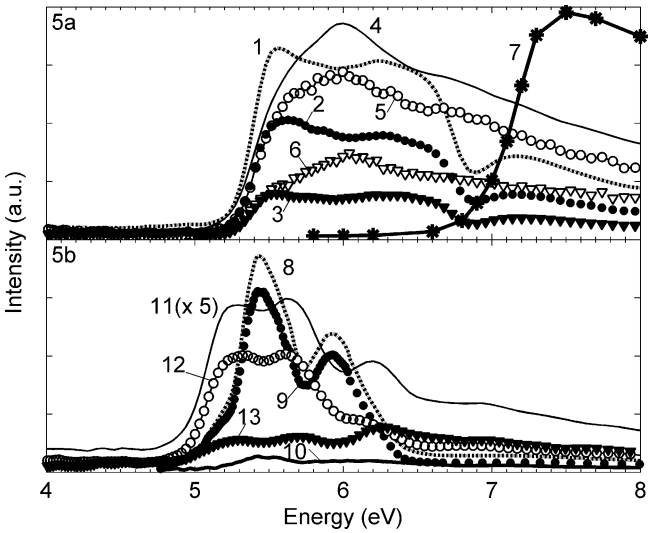

Fig. 5: Excitation spectra of (a) C12A7:Pr^{3+} (1, 2, 3) and C12A7 (4, 5, 6) monitoring emission at 3.0 eV, and creation spectrum of photostimulated luminescence for C12A7 (7) [25]; (b) C3A:Pr^{3+} monitoring emissions at 3.10 eV (11, 12, 13, 7) and at 3.94 eV (8, 9, 10). Spectra were recorded at 10 K in time-integrated mode (1, 4, 8, 11), in short- (2, 5, 9, 12; FTW: δt =1.4 ns, Δt = 7.0 ns) and in long- (3, 6, 10, 13, STW: δt =50.3 ns, Δt = 19.2 ns) time window.

These bands correspond to the direct VUV excitation to Pr^{3+} 5d levels. Two groups of emission and excitation bands competing with each other as coinciding maxima and minima indicate that there are multiple sites for Pr^{3+} ions in the C3A:Pr^{3+} sample, which agrees with the crystallographic considerations [10]. The 4.6 eV emission observed upon XUV excitation (Fig. 2d) is not present under selective VUV excitation below E_g, which means that it can be excited only via band-to-band excitation and refers to its intrinsic origin as discussed earlier. The excitation efficiency of 5d-4f emission decreases at energies larger than E_g ~6.5 eV, which shows that the energy transfer from host to Pr^{3+} $4f^15d^1$ states is inefficient. The main radiative re-

laxation channel is host-related emissions in UV that do not overlap with 4f-5d absorption bands. In the visible region, strong 4f-4f emissions were observed upon direct intracenter excitation (Fig. 4b, curve 9). The strongest band of 4f-4f emissions at 2.53 eV corresponds to $^3P_0 \rightarrow {}^3H_4$ emission. Also, weaker $^1D_2 \rightarrow {}^3H_4$ transition overlapping with $^3P_0 \rightarrow {}^3H_5$ is observed at ~ 2.03 eV. It suggests that an efficient energy transfer from $4f^15d^1$ levels to 4f $^3P_0$ state occurs, possibly via defect-related states. However, also the radiative 5d transitions populating ^3P levels are energetically possible as the fast emission bands extend to ~ 3 eV at the low energy side.

The decay curves of 5d-4f emissions in C3A:Pr^{3+} (0.25 mol%) are presented in Fig. 6. All recorded curves have a complicated nature, which can be described in the best way with a multi-exponential decay curve. The decay of 5d-4f emission under intracenter excitation of Pr^{3+} ions is characterized by the lifetimes of ~ 4.6 ns and ~ 17 ns at 10 K and ~ 2.3 ns and ~ 8 ns at 300 K, respectively. The shorter decay component can be related to the presence of competing non-radiative relaxation channels. The increase of excitation energy over E_g results in the appearance of the longer decay component of ~ 21 – 27 ns at 10 K, which is typical for the increased role of energy transfer processes to the luminescence center.

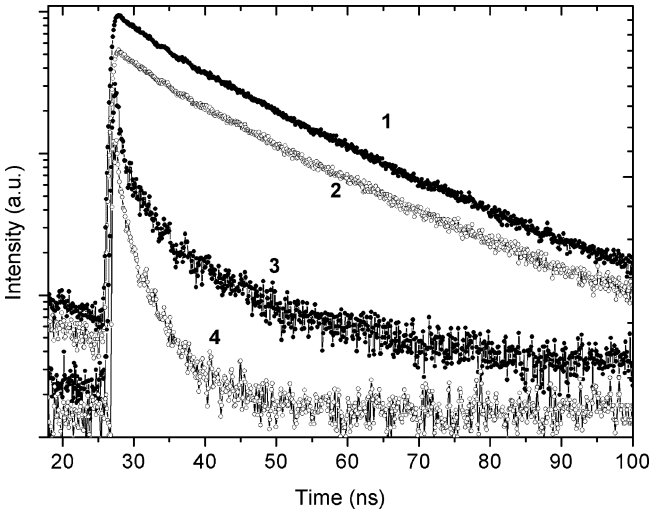

Fig. 6: Luminescence decay kinetics of Pr^{3+} 5d-4f emission (4.51 eV) in C3A:Pr^{3+} upon selective excitation of 5.44 eV (1), 6.02 eV (2), 7.75 eV (3) at 10 K; and luminescence decay kinetics of 3.92 eV emission upon excitation of 6.05 eV (4) at 300 K.

The emission spectra of C12A7:Pr^{3+} upon VUV excitation at 10 K are presented in Fig. 4a. The band gap of C12A7 was previously estimated with the photostimulated luminescence method [25] (Fig. 5a, curve 7). Under interband excitation (Fig. 4a, curve 1), low-intensity narrow 4f-4f bands of the second stage of PCE were observed. Upon 6.7 eV excitation, the broad band emission in the region of 2.0 eV to 4.5 eV was observed with complicated multicomponent decays detected in short- and long-time windows. The origin of slow decay components of this emission can be interpreted by comparing the excitation spectra of 3.0 eV emission for Pr^{3+}-doped and undoped C12A7 (Fig. 5a, curves 1, 4 respectively). The excitation onset for undoped C12A7 as well as for Pr^{3+}-doped C12A7 starts at ~ 5.0 eV. The excitation bands between 5.0 eV and 7 eV in undoped C12A7 correspond to the excitation maximum for the emissions related to the recombination of electrons and holes in the case of various extra-framework species (O^{2-}, OH^-, F^-, electrons)[7]. These O^{2-} and OH^- ions have absorption onsets at 4.7 and 5.5 eV, respectively. As seen in Fig. 5 a there are no pronounced changes in the excitation spectra at these energies. According to our previous results for Ce^{3+}-doped C12A7 [15] and to the estimation of the position of 4f5d configuration for Pr^{3+} in respect to Ce^{3+} in the same compound developed by Dorenbos [28], the 5d levels of Pr^{3+} are expected to be populated at excitation energies of ~ 5.6 eV. This region overlaps with electronic excitations related to extra-framework OH^- and O^{2-} ions [7], which are the dominating hole trapping centres in C12A7. However, the decay curves recorded indicate the presence of fast components of 4 – 40 ns typical for 5d-4f emission of Pr^{3+}. Upon excitation by 7 eV photons the contribution of low-energy emission increases (Fig. 4a curve 1). The main peak at 3 eV is a typical emission owing to oxygen encaged in pure C12A7 (see Ref. [25]) along with 4f-4f transitions forming the second stage of PCE. The ^3P levels are mainly populated by relaxation processes due to C12A7 excitations. The excitation spectra for 3 eV emission recorded in time-integrated mode, in short- and long-time window (Fig 5a, curves 1, 2 and 3, respectively) demonstrate that a drop of excitation efficiency occurs at the onset of intrinsic absorption at 6.7 eV, shown by the creation spectrum of phtostimulated luminescence (curve 7). Such behaviour is typical for 5d-4f emissions, the excited 5d electrons reaching conduction band states facilitates their escape as it has been shown for rare-earth-doped fluorides [29]. Similar excitation spectra (Fig. 5a, curves 4, 5, 6) for undoped C12A7 samples do not show such behaviour, which indicates that in the transparency range below 6.7 eV both – Pr 4f-5d absorption occurs together with excitations due to extra-framework oxygens [25]. But in case of undoped C12A7 samples the decay kinetics is in microsecond range as expected from our earlier studies.

IV. Conclusions

Time-resolved 5d-4f luminescence studies of Pr^{3+} (0.25 mol%)-doped calcium aluminates $12CaO{\cdot}7Al_2O_3$ (C12A7) and $Ca_3Al_2O_6$ (C3A) under VUV and XUV excitation were performed. For both compounds, the luminescence from $^1S_0$ level was not observed, indicating that the crystal field is strong enough, bringing 5d states to lower energies and facilitating interconfigurational 5d-4f transitions. In C3A:Pr^{3+} the broad band 5d-4f luminescence (3.5 – 4.5 eV) was observed at intracenter excitation (lifetime ~ 17 ns at 10 K) and at band-to-band excitations upon VUV and XUV radiation. In C12A7:Pr^{3+}, the situation is more complicated because of the overlap of host-related extra-framework O^{2-} ions excitations with Pr^{3+} 4f-5d states. Also, due to spectral overlap the 5d-4f luminescence is hard to distinguish from that due to extra-framework ions and host emissions of C12A7 compound. The inefficiency of energy transfer to Pr^{3+} 5d states via host excitation for both compounds, particularly in C12A7, is related to the complicated crystal structure of both hosts owing to nanoporous structure, presence

of various trapping centres, which can be recharged under ionizing radiation. Trapping centres also act as additional non-radiative and delayed radiative relaxation channels, resulting in weak emission bands of Pr^{3+} activator ions with complex decay kinetics accompanied by very low intensity of 4f-4f emissions for C12A7:Pr^{3+}. At low temperatures, C3A:Pr^{3+} has dominating 4.6 eV emission of intrinsic origin. Despite fast ns decay of 5d-4f Pr^{3+} transitions, the above-mentioned problems and modest emission intensity at room temperature does not facilitate the use of these compounds in scintillation applications. Rare-earth-doped C3A is a considerably better light emitter than C12A7-based compounds. Wide-gap (Eg ~ 6.5 eV) C3A compound has potential for optical applications, but methods to prepare it as ceramics must still be developed.

Acknowledgements

The research leading to these results has received funding from the European Community's Seventh Framework Programme (FP7/2007 – 2013) under grant agreement No. 312284, Estonian Science Foundation grant No. 8306. Also, this work has been partially supported by graduate school "Functional materials and technologies" funded by the European Social Fund under project 1.2.0401.09 – 0079 in Estonia. The authors gratefully thank Dr A. Kotlov and Dr S. Vielhauer for their help during the measurements at HASYLAB, DESY; Dr H. Mändar for assistance with the XRD measurements and A. Tõnisoo for the SEM images.

References

1 Kuck, S., Sokolska, I., Henke, M., Scheffler, T., Osiac, E.: Emission and excitation characteristics and internal quantum efficiencies of vacuum-ultraviolet excited Pr^{3+}-doped fluoride compounds, *Phys. Rev. B*, **71**, 165112, (2005).

2 Rodnyi, P.A., Mikhrin, S.B., Dorenbos, P., van der Kolk, E., van Eijk, C.W.E., Vink, A.P., Avanesov, A.G.: The observation of photon cascade emission in Pr^{3+}-doped compounds under X-ray excitation, *Opt. Commun.*, **204**, 237 – 245, (2002).

3 Srivastava, A.M., Beers, W.W.: Luminescence of Pr^{3+} in $SrAl_{12}O_{19}$: observation of two photon luminescence in oxide lattice, *J. Lumin.*, **71**, 285 – 290, (1997).

4 Sharma, S.K., Pitale, S.S., Malik, M.M., Dubey, R.N., Qureshi, M.S.: Synthesis and detailed kinetic analysis using computerized glow-curve deconvolution technique of nanocrystalline $Sr_3Al_2O_6$:Pr^{3+}. A new phosphor for UV applications, *Phys. Status Solidi* (a), **205**, 2695 – 2703, (2008).

5 Chawla, S., Kumar, N., Chander, H.: Broad yellow orange emission from $SrAl_2O_4$:Pr^{3+} phosphor with blue excitation for application to white LEDs, *J. Lumin.*, **129**, 114 – 118, (2009).

6 Matsuishi, S., Toda, Y., Miyakawa, M., Hayashi, K., Kamiya, T., Hirano, M., Tanaka, I., Hosono, H.: High-density electron anions in a nanoporous single Crystal: $[Ca_{24}Al_{28}O_{64}]^{4+}(4e^-)$, *Science*, **301**, 626 – 629, (2003).

7 Hayashi, K., Sushko, P.V., Ramo, D.M., Shluger, A.L., Watauchi, S., Tanaka, I., Matsuishi, S., Hirano, M., Hosono, H.: Nanoporous crystal $12CaO{\cdot}7Al_2O_3$: A playground for studies of ultraviolet optical absorption of negative Ions., *J. Phys. Chem. B*, **111** (8), 1946 – 1956, (2007).

8 McLeod, J.A., Buling. A., Kurmaev, E.Z., Sushko, P.V., Neumann, M., Finkelstein, L.D., Kim, S.-W., Hosono, H., Moewes, A.: Spectroscopic characterization of a multi-band complex oxide: insulating and conducting cement $12CaO{\cdot}7Al_2O_3$, *Phys. Rev. B*, **85**, 045204, (2012).

9 Sushko, P.V., Shluger, A.L., Hayashi, K., Hirano, M., Hosono, H.: Hopping and optical absorption of electrons in nano-porous crystal $12CaO{\cdot}7Al_2O_3$, *Thin Solid Films*, **445**, 161 – 167, (2003).

10 Mondal, P., Jeffrey, J.W.: The crystal structure of tricalcium aluminate, $Ca_3Al_2O_6$, *Acta Cryst.*, **B31**, 689 – 697, (1975).

11 Alonso, J., Rasines, I., Soubeyroux, J.: Tristrontium dialuminate Hexaoxide: an intricate superstructure of perovskite, *Inorg. Chem.*, **29**, 4768 – 4771, (1990).

12 Schiffbauer, D., Wickleder, C., Meyer, G., Kirm, M., Stephan, M., Schmidt, P.: Crystal structure, electronic structure, and luminescence of Cs_2KYF_6 : Pr^{3+}, *Z. Anorg. Allg. Chem.*, **631**, 3046 – 3052, (2005).

13 Wang, D., Liu, Y.X., Liu, Y.C., Xu, C.S., Shao, C.L., Li, X.H.: Preparation and visible emission of Er-doped $12CaO{\cdot}7Al_2O_3$ powder, *J. Nanosci. Nanotechnol.*, **8**, 1458 – 1463, (2008).

14 Zhang, P., Xu, M., Liu, L., Li, L.: Luminescent properties of $Sr_3Al_2O_6$: eu, pr prepared by sol-gel method, *J. Sol Gel Sci. Technol.*, **50**, 267 – 270, (2009).

15 Tõldsepp, E., Avarmaa, T., Denks, V., Feldbach, E., Kirm, M., Maaroos, A., Mändar, H., Vielhauer, S.: Synthesis and luminescence properties of Ce^{3+} doped nanoporous $12CaO{\cdot}7Al_2O_3$ powders and ceramics, *Opt. Mater.*, **32**, 784 – 788, (2010).

16 Xue, L.L., Liu, Y.X., Xu, C.S., Liu, Y.C., Zhao, C.J., Zhang, X.T.: Characterization and optical transition in tb-doped $12CaO{\cdot}7Al_2O_3$ Powders, *J. Nanosci. Nanotechnol.*, **10**, 2125 – 2130, (2010).

17 Zhu, H., Liu, Y., Yan, D., Yan, X., Liu, C., Xu, C.: White luminescence of Dy^{3+} ions doped $12CaO{\cdot}7Al_2O_3$ nanopowders under UV light excitation, *J. Nanosci. Nanotechnol.*, **11**, 9958 – 9963, (2011).

18 Ianos, R., Lazau, I., Pacurariu, C., Barvinschi, P.: Fuel mixture approach for solution combustion synthesis of $Ca_3Al_2O_6$ powders, *Cem. Concr. Res.*, **39**, 566 – 572, (2009).

19 Kim, S., Miyakawa, M., Hayashi, K., Sakai, T., Hirano, M., Hosono, H.: Simple and efficient fabrication of room temperature stable electride: Melt-solidification and glass ceramics, *J. Am. Chem. Soc.*, **127**, 1370 – 1371, (2005).

20 Kim, S., Matsuishi, S., Miyakawa, M., Hayashi, K., Hirano, M., Hosono, H.: Fabrication of room temperature-stable $12CaO{\cdot}7Al_2O_3$ electride: a review, *J. Mater. Sci. – Mater. El.*, **18**, S5 – S14, (2007).

21 Kajihara, K., Matsuishi, S., Hayashi, K., Hirano, M., Hosono, H.: Vibrational dynamics and oxygen diffusion in a nanoporous oxide ion conductor $12CaO{\cdot}7Al_2O_3$ studied by O-18 labeling and micro-raman spectroscopy, *J. Phys. Chem. C*, **111**, 14855 – 14861, (2007).

22 Zimmerer, G.: SUPERLUMI: A unique setup for luminescence spectroscopy with synchrotron radiation, *Radiat. Measur.*, **42**, 859 – 864, (2007).

23 Kirm, M., Lushchik, A., Lushchik, C., Vielhauer, S., Zimmerer, G.: Luminescence of pure and doped Al_2O_3 and MgO single crystals under inner-shell excitation, *J. Lumin.*, 102 – 103, 307 – 312, (2003).

24 Babin, V., Feldbach, E., Kirm, M., Makhov, V.N., Vielhauer, S.: Deep VUV scintillators for detectors working in cryogenic environment, *IEEE Trans. Nucl. Sci.*, **55**, 1437 – 1444, (2008).

25 Feldbach, E., Denks, V.P., Kirm, M., Kunnus, K., Maaroos, A.: Intrinsic excitons in $12CaO{\cdot}7Al_2O_3$, *Radiat. Meas.*, **45**, 281 – 283, (2010).

26 Vedda, A., Fasoli, M., Nikl, M., Laguta, V.V., Mihokova, E., Pejchal, J., Yoshikawa, A., Zhuravleva, M.: Trap-center recombination processes by rare earth activators in $YAlO_3$ single crystal host, *Phys. Rev. B*, **80**, 045113 – 1-9, (2009).

[27] Lushchik, A., Kirm, M., Lushchik, C., Martinson, I., Zimmerer, G.: Luminescence of free and self-trapped excitons in wide-gap oxides, *J. Lumin.*, **87 – 89**, 232 – 234, (2000).

[28] Dorenbos, P.: The 5d level positions of the trivalent lanthanides in inorganic compounds, *J. Lumin.*, **91**, 155 – 176, (2000).

[29] Makhov, V., Khaidukov, N., Kirikova, N., Kirm, M., Krupa, J., Ouvarova, T., Zimmerer, G.: VUV emission of rare-earth ions doped into fluoride crystals, *J. Lumin.*, **87 – 89**, 1005 – 1007, (2000).